An experimental and theoretical study of the structural ordering of the PTB7 polymer at a mesoscopic scale

An experimental and theoretical study of the structural ordering of the PTB7 polymer at a mesoscopic scale

Pavel Urbánek[a,*], Ivo Kuřitka[a], Jakub Ševčík[a], Jana Toušková[b], Jiří Toušek[b], Vojtěch Nádaždy[c], Peter Nádaždy[c], Karol Végso[c], Peter Šiffalovič[c], Radka Rutsch[b], Michal Urbánek[a]

[a]Centre of Polymer Systems, University Institute, Tomas Bata University in Zlin, tř. T. Bati 5678, 760 01, Zlín, Czech Republic
[b]Charles University, Faculty of Mathematics and Physics, Department of Macromolecular Physics, V Holešovičkách 2, 180 00, Prague, Czech Republic
*[c]Institute of Physics, Slovak Academy of Sciences, Dúbravská cesta 9, 845 11, Bratislava, Slovak Republic**
Corresponding author: E-mail address: urbanek@utb.cz

HIGHLIGHTS

- The physical properties of PTB7 films are governed by chains structural ordering.
- There exists a thickness threshold in all of investigated aspects of the films at about 130nm.
- Theoretical model was used for description of driving forces causing observed phenomena.
- The driving forces are conclusively associated with thickness threshold.

ARTICLE INFO

Keywords: Conjugated polymers, low band-gap, thickness dependences

ABSTRACT

Our extensive study based on optoelectronic and electric measurements (which consisted of: UV–Vis absorption, photoluminescence, surface photovoltage measurement, charge extraction by linearly increasing voltage, and energy-resolved electrochemical impedance spectroscopy) revealed the fundamental role of the thickness of the formation of intra- and interchain interaction in poly({4,8-bis[(2-ethylhexyl)oxy]benzo[1,2-b:4,5-b']dithiophene- 2,6-diyl}{3-fluoro-2-[(2-ethylhexyl)carbonyl]thieno[3,4-b]thiophenediyl}) (PTB7) films. We have shown that the final optoelectronic and electronic properties of PTB7 films are governed by the structural ordering development of the transition from nano-to submicroscale. The ordering of polymer chains and competition between the formation of J- and H-aggregates results in a non-trivial dependence of luminescence, exciton diffusion length, transport band gap, and defect concentration. According to a theoretical analysis, the driving forces responsible for the observed phenomena are associated with the thickness threshold dependence of the thin film drying mode which can proceed with or without the polymer skin formation on the surface of forming
film.

1. Introduction

The need to develop inexpensive renewable energy sources continues to stimulate new approaches for the production of efficient, low- cost photovoltaic devices **[1]**. Improving the performance of organic solar cells requires the understanding and mastering of a materials' behaviour and the controlling of interfaces between organic — organic and organic — inorganic materials, the design of the morphology of the active layer, as well as the molecular engineering of organic materials, and last but not least, the optoelectronic properties must be adjustable to the desired parameters **[2]**. Based on the latter approach, several donor — acceptor (D-A) copolymers with a low band gap and a suitable HOMO (highest occupied molecular orbital) level matching to fullerene are synthesized **[3-5]**.

While extensive studies on how to improve the power conversion efficiency (PCE) of organic photovoltaic (OPV) devices have focused on the influence of the synthesis and molecular structure of conjugated polymers on both the photophysics and devices' performance **[5-8]**, there still exists a contradiction between the described behaviour in thick films and the prevalent experience gathered from the solution and thin films. The results must be more matched together to obtain a complex and consolidated view of the problem. Moreover, the effects of a second order are often manifested in experimental observations, and the photophysical properties and final device performance are found tobe extremely sensitive to processing parameters such as solvent choice, polymer solution concentration, spin coating conditions, annealing and the heat treatment temperature program. All of these parameters are considered to influence the polymer chain orientation and the structure of the obtained solid films **[9-11]** but are still discussed separately.

An explanation of the differences between the behaviour of conjugated polymers in the solution and in the form of thin and thick films can be found with the help of the intra- and intermolecular J- and H— aggregates concept as described in Refs. **[12-15]**. This phenomenon of structural ordering, introduced by Kasha and coworkers **[16-18]**, plays a significant role in understanding the optoelectronic processes following the event of photon absorption. The electronic interactions between molecules results in a red- or blue-shift of the main absorption peak in J- or H— aggregates respectively, in comparison to the isolated molecules in solution. The luminescence emission is also influenced, besides the bathochromic shift due to the J-aggregation and the hyp- sochromic shift observable for H-aggregates, the plane to plane stacking of H-aggregates decreases the emission intensity in comparison to the non-aggregated state. Both forms of overlap interactions induce a delocalisation of the excited states or Frenkel excitons and increase the transport properties **[19]**. Indeed, recent works suggest that single chains of emissive conjugated polymers behave photophysically like J- aggregates due to their linear arrangement of conjugated mer units. The photophysics of the conjugated polymer n-stacks of the polymer chains is then determined by a competition between a J-favouring intrachain interaction and a H-favouring interchain interaction. Nevertheless, the cause of why J- or H-aggregates prevail in solid thin films is still not well explained and sufficiently discussed. Some research works describe a relationship among the structure, morphology, the polymer chain aggregation and the optoelectronic properties of conjugated polymers **[2,12**, and **20]**]. The studies are performed on only thick (thickness about microns) or thin (thickness about tens of nanometers) films or on the polymers in solution. If the sample thickness is varied on the scale from thin to thick, any unexpected (non-trivial) non-linear dependences and transitions between values typical for the two extremes can be measured for characteristic physical properties. A specific threshold in optoelectronic behaviour can be observed between nano- and microscale, situated at about several hundred nm as shown in our previous work **[21,22]** on thin films as well as reported for physical parameters of photovoltaic diodes (conjugated polymer-fullerene based heterojunction diodes) by other authors **[23]**. The effect of the polymer chain conformational disorder was also investigated in theoretical studies **[24,25]**. Also, the dielectric

properties of insulating films (polyimides) are found to be sensitive to the polymer chain orientations' dependence on the thickness scale threshholding between one hundred and one thousand nanometers **[26]**. This effect seems to exist beside other minor (less important) effects of processing history and the chosen technology of the sample preparation. Together with reports on the mechanical properties **[27,28]**, the term 'mesoscale effect' can be coined to refer to this phenomena.

In this work, we present an extensive study of the optoelectrical, the electrical and the structural properties of the polymer PTB7, measured by various independent techniques, namely UV-VIS and PL spectroscopy, the SPV method, CELIV and the energy-resolved electrochemical impedance spectroscopy and grazing-incidence wide-angle X-ray scattering (GIWAXS). The explanation integrates the concept of J and H aggregates into the mesoscale effect framework. In line with previous reports, it seems that the mesoscale effect can be relevant for films of conjugated polymers with thicknesses varying between nano- and micrometers. Moreover, we believe that this general concept pertains to the use of conjugated polymers in real applications too, because it allows us to understand and predict more precisely the film thickness dependence of properties such as the exciton diffusion length, the exciton recombination, charge carrier transport and chain degradation (See **Fig. 1**).

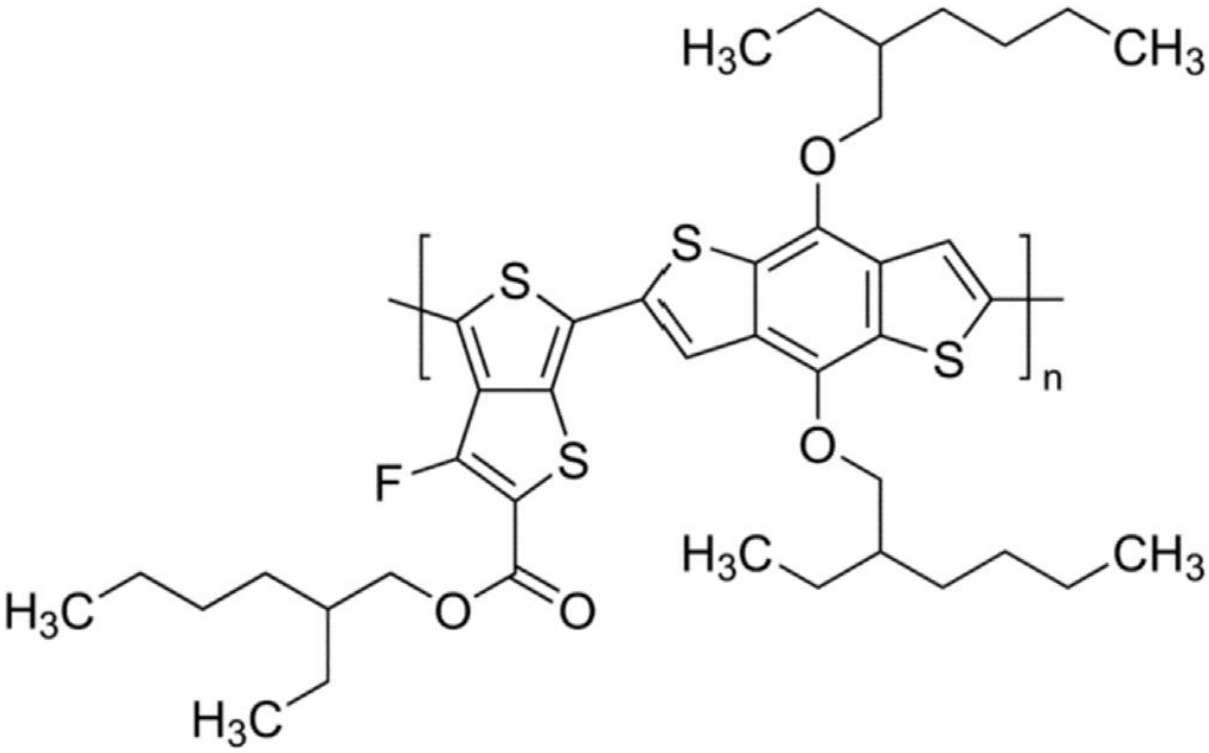

Fig. 1. Structure of PTB7 polymer.

2. Experimental

2.1. Sample preparation

A series of spin coated thin films were prepared from a solution of poly({4,8-bis[(2-ethylhexyl)oxy]benzo[1,2-b:4,5-b']dithiophene-2,6-diyl}{3-fluoro-2-[(2-ethylhexyl)carbonyl]thieno [3,4-b]thiophene- diyl}) (PTB7) in the mixture of solvents (toluene and chloroform). The polymer PTB7 was obtained fromSigma Aldrich; Mw = 80,000-200,000. The polymer solutions were cast onto quartz glass, glass/ITO and n-doped silicon substrates using the spin coater Laurell WS-650-MZ-

23NPP with a rotation speed varying from 4500 to 1000 rpm. Two solution concentrations were used for this process, 10mgmL^{-1} and 20mgmL^{-1}, respectively. After the deposition, the films were dried at 100 °C. The whole process of the sample preparation was performed in a nitrogen atmosphere in a glove box.

2.2. Material characterization

The thickness of films, measured by a mechanical profilometer Dektak XT-E (Bruker) with a 1 nm resolution, ranged from 40 nm to 300 nm. The absorption spectra were measured by the Lambda 1050 UV/VIS/NIR spectrometer from Perkin Elmer. The optical band gaps were determined using a Tauc plot. The fluorimeter FSL 920 from Edinburgh Instruments (UK) was used for the measuring of PL spectra. The PL spectra were taken in a vacuum (pressure 1 Pa) ensured by the cryostat Optistat DN-V (LN2), Oxford Instruments at room temperature.

2.3. Surface photovoltage

The surface photovoltage was measured in the arrangement shown in **Fig. 2**.
The samples were illuminated from the side of the bulk. In this case, the field of the SCR dissociating the excitons is formed at the top surface of the sample. The excitons diffusing in the bulk generate a diffusion current after the dissociation. A drift current is the result of the dissociation of the excitons photogenerated in the SCR.

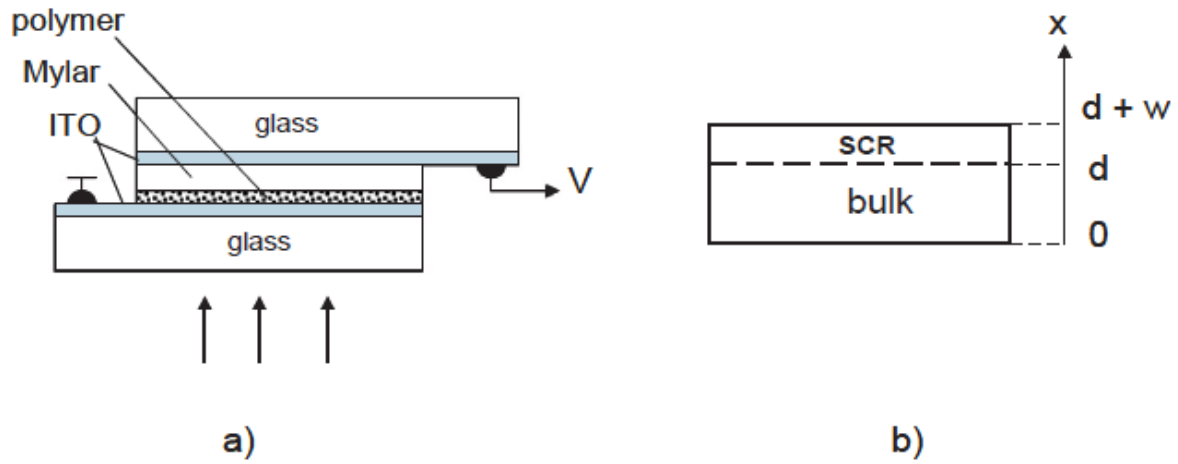

Fig. 2. a) the arrangement for the surface photovoltage measurement; b) the structure of the polymer layer: *d* is the thickness of the bulk; *w* is the thickness of the space charge region (SCR).

The processes of the diffusion and of the drift are described e.g. in our previous article **[21]**. The diffusion equation for the calculation of the diffusion current is solved with the following boundary conditions: at the ITO/bulk interface a recombination of excitons is introduced by the relation

$$Dd\Delta n(x)/dx|_{x=0} = s\Delta n(0) \qquad (1)$$

the assumption of a perfect sweeping of excitons at the SCR/bulk interface leads to

$$\Delta n(d) = 0 \qquad (2)$$

The diffusion equation yields the concentration of the photogenerated excitons Δ*n(x)* at the depth x, *s* is the surface recombination velocity, *d* is the thickness of the neutral bulk, and *D* is the exciton diffusion coefficient. The diffusion current J_{diff} is proportional to the derivative $d\Delta n(x)/dx$ at the SCR/bulk interface. The current density, J_{drift} from the SCR is given by the integration of the exciton photogeneration rate over the distance *w* where the dissociation of the ex- citons takes place. Losses by possible recombination in the space charge region are characterized by the gain factor (g). The total photocurrent is a sum of the diffusion current from the bulk and the drift current from the SCR.

$$J = J_{diff} + J_{drift} \quad (3)$$

The calculations of these currents are shown in Ref. [**21**] or in Ref. [**29**]. The experimentally verified linear relation between the photovoltage and the light intensity leads to the proportionality between the photovoltage *V* and the photogenerated current density *J*.

$$V \sim J \quad (4)$$

2.4. CELIV method

A charge extraction by linearly increasing voltage (CELIV) method **[30,31]** was used for measuring the mobility of the polymer within the study. The measurement was done in the dark, without illumination. The set up consists of an oscilloscope (OWON DS 7102 V), an arbitrary function generator (Agilent 33250 A) and a holder with the sample. For the CELIV measurement Au/p-PTB7/n-Si/In, a structure was created with a p-PTB7/n-Si blocking junction or an Al/LiF/PTB7/ITO Schottky diode with an Al/LiF blocking electrode. A linearly increasing voltage pulse is applied and the current response over time is measured by the oscilloscope. For the evaluation of the mobility, the offset voltage originating in the difference of the electrode work functions was included. The mobility was calculated using the usual relation given in Ref. **[31]**.

2.5. Energy-resolved electrochemical impedance spectroscopy

The novel spectroscopic method, Energy-resolved electrochemical impedance spectroscopy (ER-EIS) [**32**], is used for the measurement of the density of states (DOS). The ER-EIS method is based on the measurement of the charge transfer resistance, *R*ct, of a semiconductor/ electrolyte interface at a frequency where the redox reactions determine the real component of the impedance. The DOS function *g(E)* in the semiconductor at the electrochemical potential $Ep,_{re}dox = eU$ can be expressed in terms of the *R*ct measured at the applied voltage *U* as **[32,33]**.

$$g(E_{F,redox} = eU) = \frac{1}{e^2 k_{et}[A] S R_{ct}} \quad (5)$$

where *e* is the elementary charge, *k*et is the charge-transfer rate constant, [*A*] is the concentration of the electrolyte redox (donor/acceptor) type in the interphase region of the solid/liquid contact, and *S* is the sample area. The reciprocal value of the R_{ct} resistance measured as a response to the harmonic perturbation with the amplitude d*U* and an appropriate frequency provides direct information about the electronic DOS at the energy adjusted using an external voltage.

The impedance/gain-phase analyzer Solartron analytical, model 1260 was used for the ER-EIS experiment. The frequency was set to 0.5 Hz, the amplitude of AC voltage was 100 mV, and the average sweep rate of the DC voltage ramp was 10 mV/s. The measurements were performed in a

glove box with a protective N_2 atmosphere (oxygen and moisture below 20 ppm and 2 ppm, respectively), using a common three-electrode electrochemical cell with a volume of about 200 μL. The solution of 0.1 M TBAPF6 in acetonitrile was used as the supporting electrolyte. The potential of the working electrode with respect to the reference Ag/AgCl electrode was controlled by means of the potentiostat. Pt wire was used as the counter electrode. The potential recorded with respect to the reference Ag/AgCl electrode can be recalculated to the local vacuum level assuming the Ag/AgCl energy vs. vacuum value of 4.66 eV.

The tested thin films were found to be insensitive to the swelling by the used solvent system for at least 10 min, as verified by the photoluminescence spectra measurement on the immersed control samples.

2.6. Grazing-incidence wide-angle X-ray scattering (GIWAXS)

Grazing-incidence wide-angle X-ray scattering (GIWAXS) experiments were measured on a custom-designed Nanostar system (Bruker, Germany) equipped with a liquid-metal jet X-ray source emitting at the wavelength of 1.34 A. All samples were measured in grazing-incidence geometry at the incident angle of 0.2°. The scattered X-ray radiation was captured by an imaging plate at a distance of 194 mm.

3. Results and discussion

3.1. PL study

Fluorescence spectroscopy can be used as a useful tool for the structure characterization of the thin polymer films **[22,34]**. In the case of PTB7, the Stoke's shift is large enough, so the material does not absorb at the emission maximum wavelength at all. Thus reabsorption cannot distort the PL measurements. The representative normalized emission PL spectra of thin PTB7 films with different thicknesses are depicted in **Fig. 3**. The emission spectra bear information on the nature of the excited states that undergo radiative recombination, therefore, the dependence of the emission properties on the thickness can be interpreted with respect to the microphysical structure of the investigated polymer films.

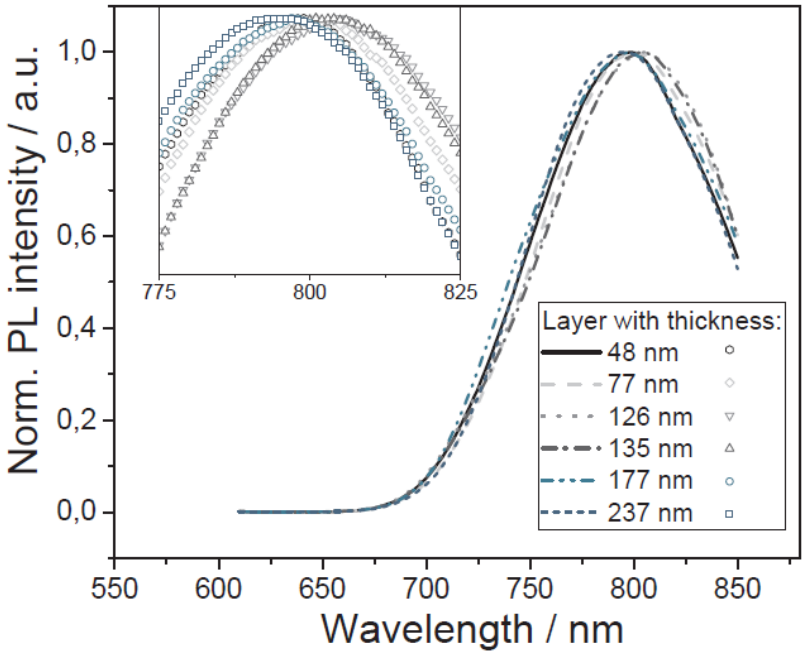

Fig. 3. The representative emission spectra of thin PTB7 films, Xexc = 680 nm.

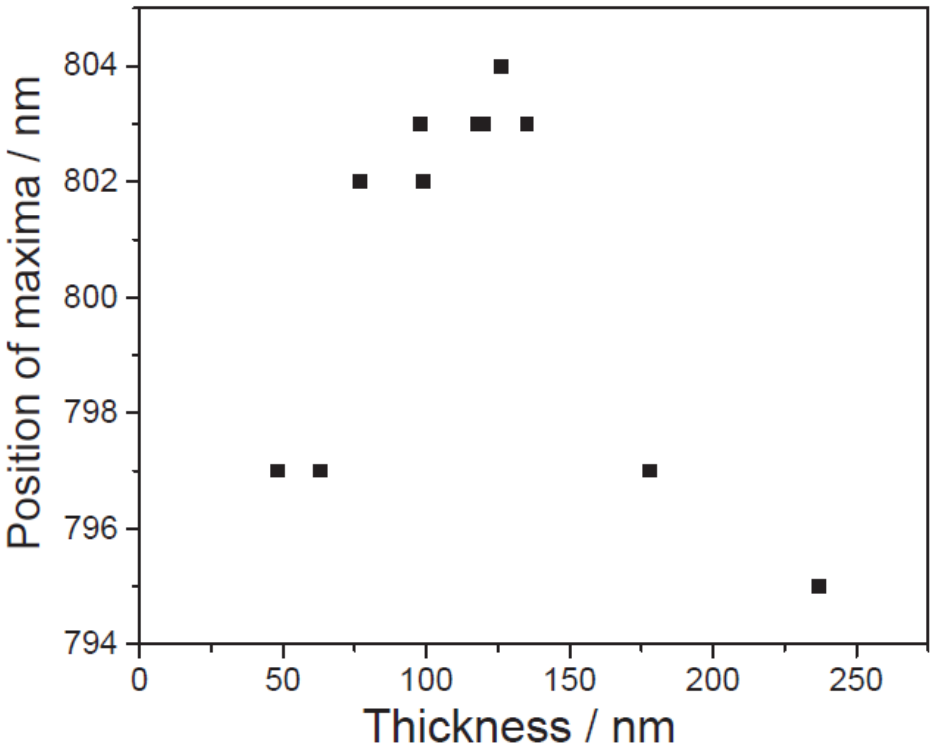

Fig. 4. The dependence of the position of emission maxima on the layer thickness, X_{exc} = 680 nm.

The shifts of PL maxima in the emission spectra (shown in Fig. 4) reveal that both the intrachain effective conjugation length and the interchain n-interactions are changed by increasing the film thickness with the threshold behaviour at a thickness of about 130 nm. The emission spectra present one dominant peak at about 800 nm. For films with a thickness from 50 nm to 126 nm, the emission maxima are red shifted with increasing thickness, indicating an enhancement of the effective

conjugation length. The very thin films (50 nm) do not have enough material to build up an ordered structure with a pronounced interchain interaction hence J-aggregates arise preferentially. However, with increasing the thickness (film thickness above 100 nm) polymer chains can be better aligned in stacks which can gradually contribute to the increase of the importance of the H-type interchain interaction although the planarisation of the chains and a further increase in the effective conjugation length may also lead to the energy lowering which supports the J-aggregate formation. Hence, a competitive effect of the J- and H— aggregates is manifested [**2**], which was observed and described also for the other materials **[21,22,35**, and **36]**]. As a result, both contributions seem to be balanced in the transition region between the thickness of 100 and 130 nm.

Once the film is thick enough (more than 130 nm), the red emission shift is stopped and the blue shift appears with the next increasing thickness. This phenomenon can be explained by a Coulombic interchain coupling and so called HJ-aggregates, whereas the effect of the n- stacking of chains can prevail **[13]**.

3.2. Exciton diffusion length and carrier mobility

The conformational order of the individual polymer chains as well as the ordering of the n-conjugated polymer chains in stacks can influence the exciton diffusion length. Therefore, our modified SPV method [**29**] can be used as an advantage because it allows determining the diffusion length by measuring of a single sample. So, it is sensitive to the changes of the diffusion length varying with thickness. In the arrangement where the sample is illuminated from the bulk side (see **Fig. 2**) the SPV signal corresponds to the spectral dependence of absorbance. For the SPV evaluation, measurement of absorbance (to find the absorption coefficients) and reflectance data is necessary. Multiple reflections of incoherent light from both surfaces are included in the theory. The important parameters of the SPV spectra, namely the diffusion length of excitons, bulk thickness, space charge region thickness and gain factor were obtained by fitting the theory to the experiment. In our case, the surface recombination velocity practically did not influence the spectra.

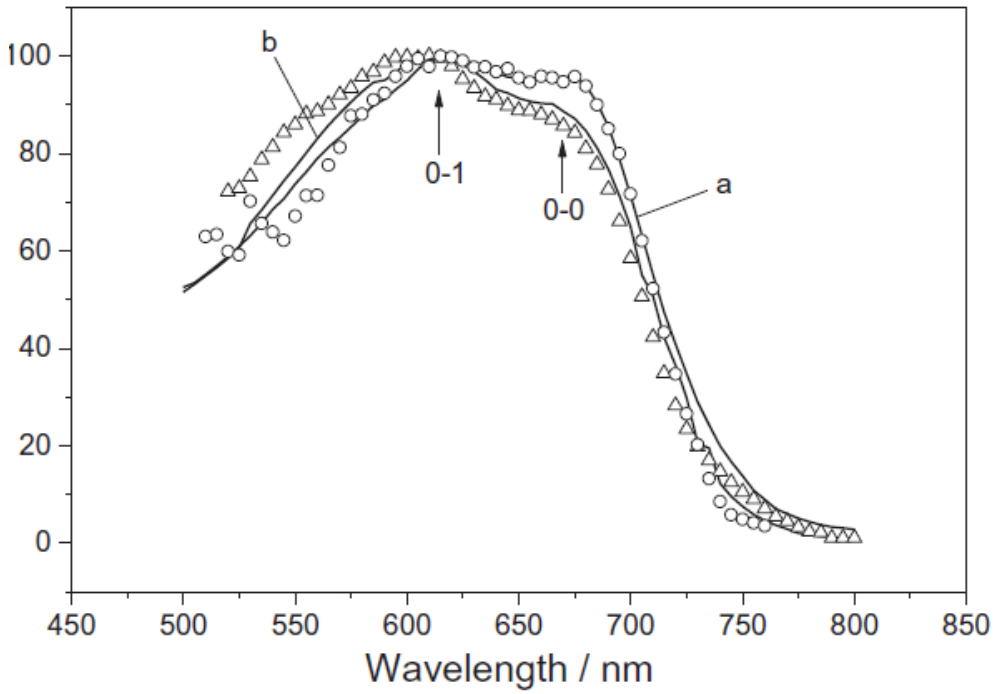

Fig. 5. The normalized surface photovoltage spectra of the PTB7 samples with thicknesses of 250 nm (circles) and 149nm (triangles). Theoretical curves (lines) were fitted to the experimental points (line "a" for circles and line "b" for triangles) with a diffusion length of L = 15 nm and 12 nm, respectively.

The exciton diffusion length was determined for the PTB7 layers with thicknesses ranging from 50 to 250 nm. **Fig. 5** displays an example of the experimental and theoretical photovoltage spectra. The theoretical curves well fitted to the experimental points provide the diffusion length of excitons.

In **Fig. 5**, the peak corresponding to a 0-0 optical transition is well seen for the sample with a thickness of 250 nm. Only a shoulder can be found in the experimental curve of the 149 nm thick sample. On the other hand, the peak 0-1 is evident in both spectra. The sample with a thickness of 136 nm shows characteristics similar to that of the 149 nm sample.
All of the studied samples showed the positions of 0-1 and 0-0 peaks at 614 nm and 660 nm, respectively, except for the samples with thicknesses of 136 nm and 149 nm in which the maximum for the 0-0 transition is not precisely defined and therefore the positions of the inflection point on the shoulders were used to read the value of the signal intensity. The (0-0/0-1) peak ratio (Fig. 6) is in the range from 0.87 to 0.90 for the samples thinner than 200 nm and thicker than 100 nm. A decrease of the ratio is seen for the samples with thicknesses thinner than 100 nm. Simultaneously, the dependence of the exciton diffusion length on the layer thickness is shown in Fig. 6, whereas the transition region is situated between 100 and 200 nm.

It is possible that for small thicknesses of up to about 100 nm, structural ordering of polymer chains is small, i.e. the chains do not create long segments for long exciton diffusion.

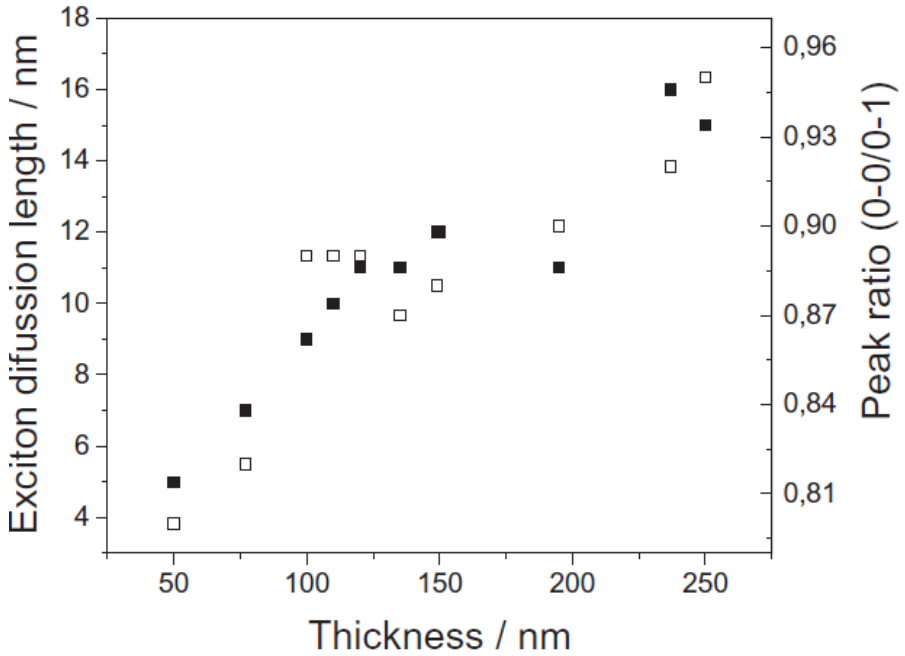

Fig. 6. The dependence of the exciton diffusion length (full symbols) and the peak ratio (0-0/0-1) in the SPV spectra (empty symbols) on the layer thickness.

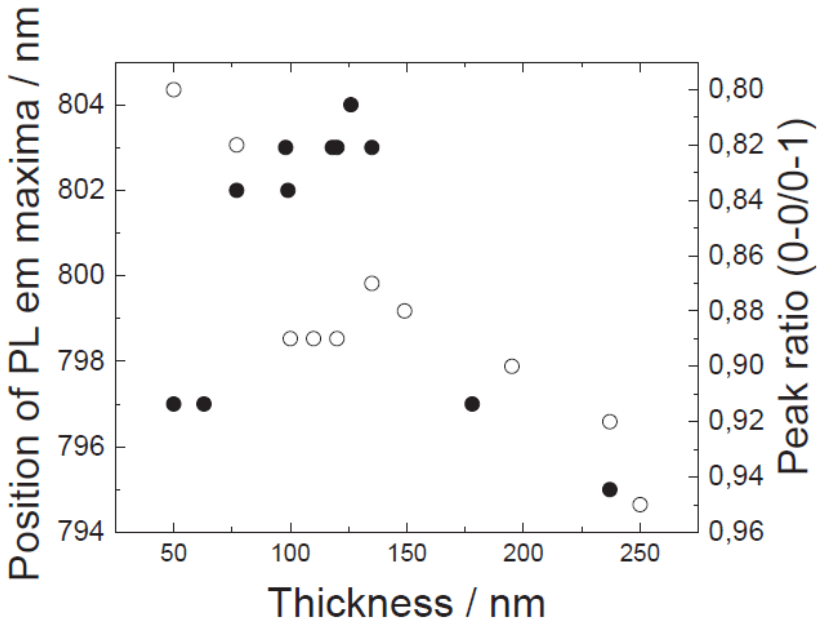

Fig. 7. The correlation of the position of luminescence emission maxima (full symbols) excited by λ_{exc} = 680 nm, and (0-0/0-1) the peak ratio (empty symbols) obtained by the SPV signal analysis, plotted against the film thickness.

In case of films with thicknesses over 100 nm there is a relatively good structural ordering along the individual polymer chains which increases the effective conjugation length and leads to quite a high exciton diffusion length and higher $I_{0\text{-}0}/I_{0\text{-}1}$ peak ratio. In the 100-200 nm thickness region the ordering is changed and both, exciton diffusion length and the $I_{0\text{-}0}/I_{0\text{-}1}$ ratio are not linear dependent on thickness. The increasing tendency of thickness dependence of the exciton diffusion length in this region slows and the structure ordering probably changes. Over the thickness of 200 nm, the exciton diffusion length and $I_{0\text{-}0}/I_{0\text{-}1}$ ratio increase again. We suggest that the steep increase of the diffusion length indicates a higher degree of the ordered structure and possibly interchain interaction or the

H-J aggregates formation. Similar conclusions were reported here **[13,37]**. A good correlation between the results obtained from the PL and SPV measurements is shown in **Fig. 7** too.

The charge carrier mobility of the thin PTB7 films increases by increasing the film thickness as shown in **Fig. 8**. Also in this case, the increase of mobility is not linear at all. The region 100-150 nm seems to be a critical thickness interval, above this, the increase is slowed down.

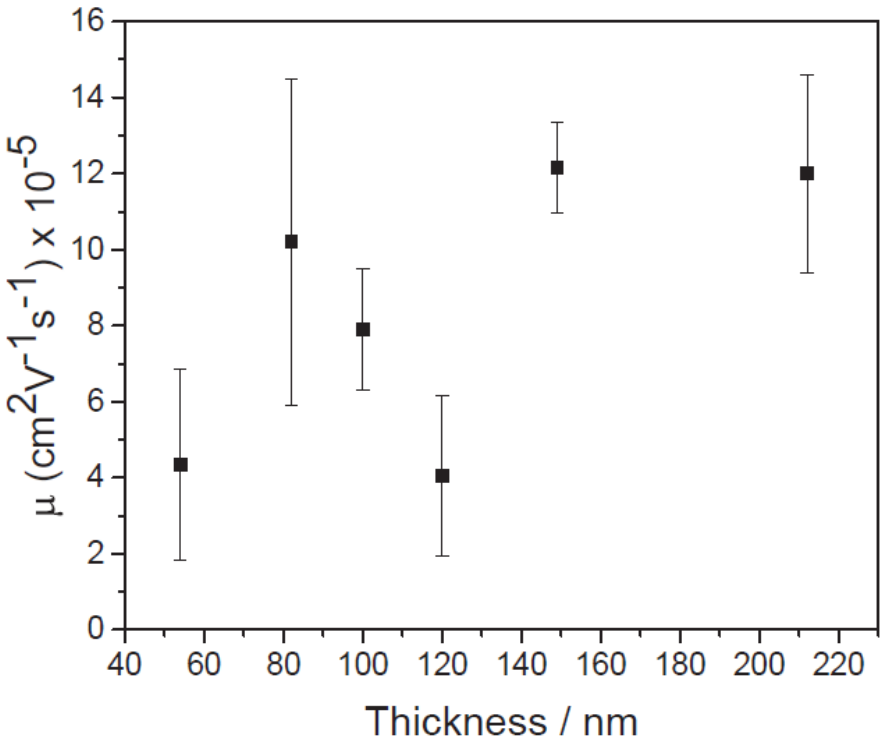

Fig. 8. The charge carrier mobility of PTB7 samples as a function of their thickness.

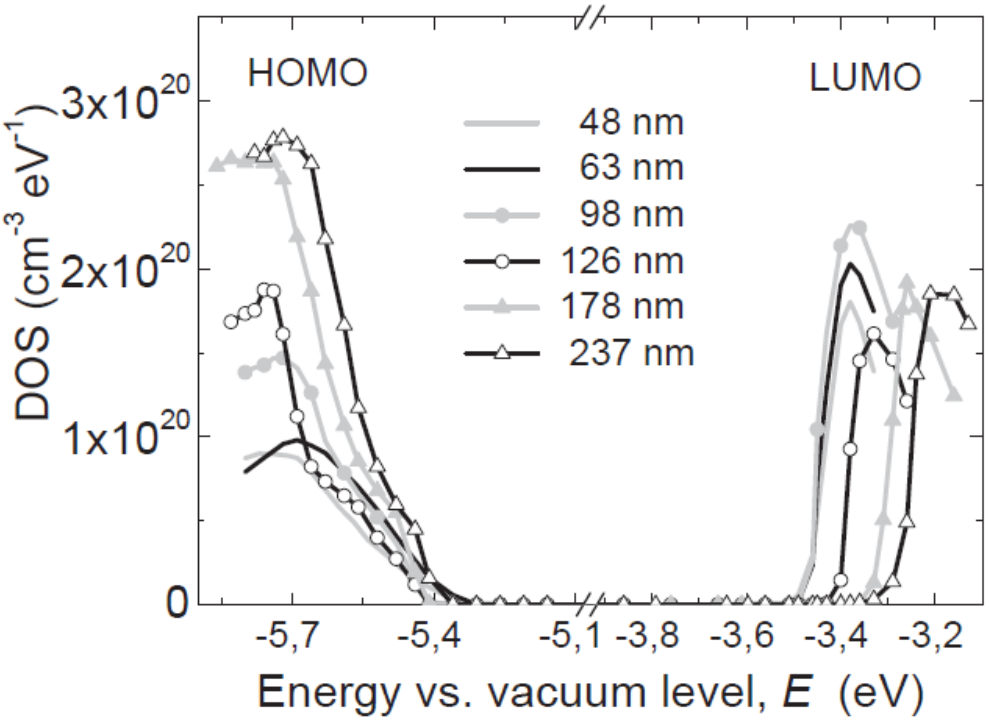

Fig. 9. The representative ER-EIS spectra of the PTB7 films with different thicknesses in linear scale.

To summarize partially: In the investigated PTB7 films, all of the properties related to the absorption, exciton diffusion length, photoluminescence and charge carrier mobility are strongly influenced by the layer thickness. Moreover, there exists a thickness threshold in all of the examined aspects of the films at the thickness region from 100 to 150 nm.

3.3. Energy-resolved electrochemical impedance spectroscopy

The thickness dependence of the DOS measured by the ER-EIS method is depicted in **Figs. 9** and **10**. This DOS dependence on a linear scale (**Fig. 9**) reveals a widening of the band gap mainly due to the shift of the LUMO to lower the energies with respect to the vacuum level. The band onsets were used for the electrochemical (transport) gap determination. It was demonstrated on the P3HT that this approach is equivalent to the techniques of cyclic and linear sweep voltammetries **[38]**. The dependence of the transport and optical band gaps on the layer thickness is shown in **Fig. 11**. The transport gap of about 1.75 eV for the thinnest layer increases up to 2.00 eV for the layer thicknesses around 100 nm and then a tiny increase up to 2.05 eV is observed for thicker layers. On the other hand, no apparent change of the optical gap is visible. Small variations in its values correspond with changes in wavelength lower than 5 nm.

The DOS spectra in the logarithmic scale in **Fig. 10** reflect the dynamic range between the DOS of the HOMO and LUMO bands and defect the density of the states in the band gap. We calibrated the DOS axis, taking into account the concentration at the HOMO and LUMO in the order of 10^{20} $cm^{-3}eV^{-1}$ **[39]**. The defect DOS in the gap is monotonously distributed and its concentration varies from 10^{15} - $10^{16}cm^{-3}eV^{-1}$ in the studied thickness range of the PTB7 layers.

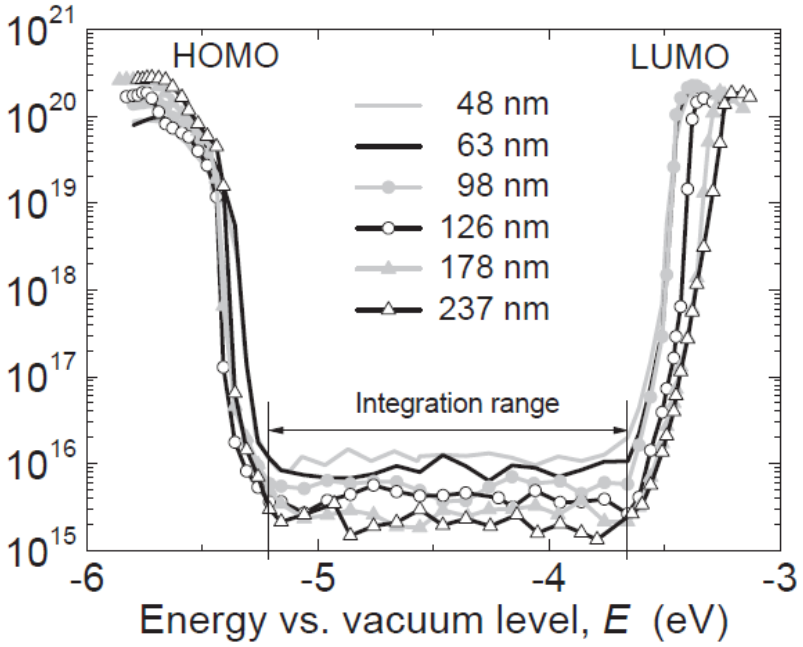

Fig. 10. The representative ER-EIS spectra of the PTB7 films with different thicknesses in log scale.

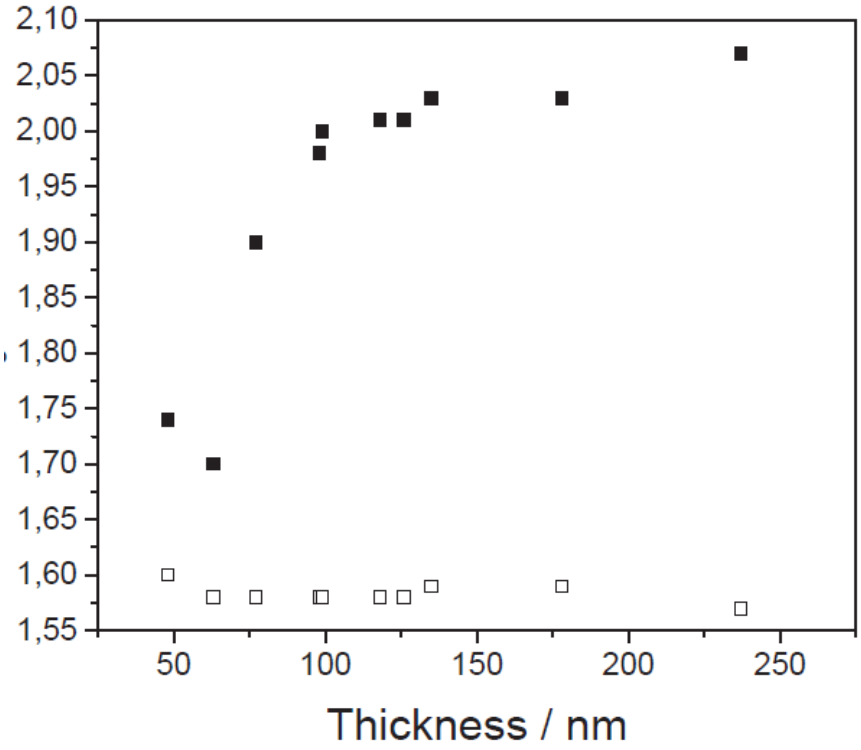

Fig. 11. The dependences of the transport (full symbols) and the optical (empty symbols) band gaps on the layer thickness.

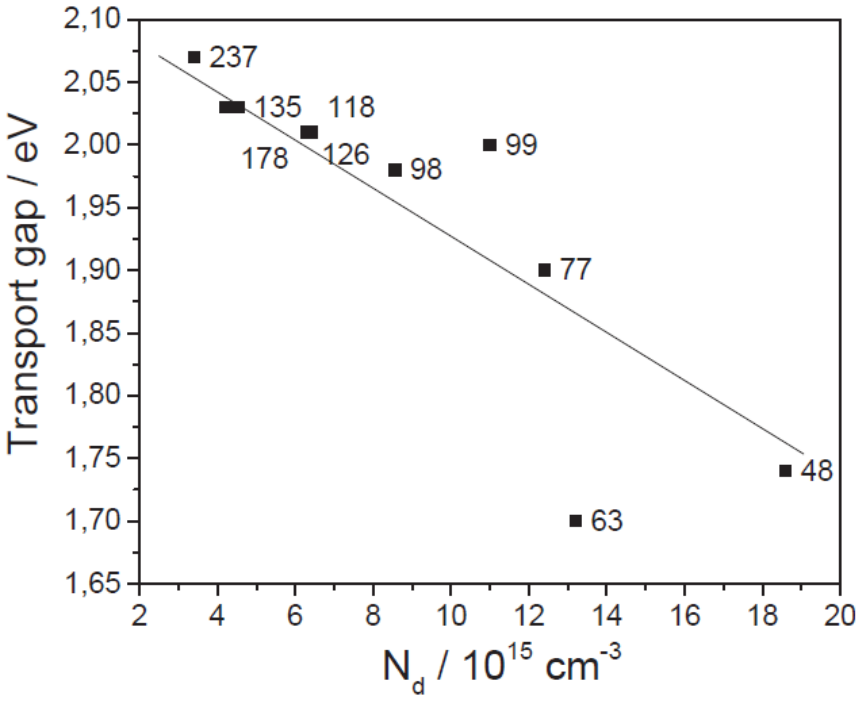

Fig. 12. The dependence of the transport gap width on the defect concentration (N_d), labeled with the sample thicknesses in nm.

The increase of the transport band gap depends inversely on N_D, calculated in the energy interval marked in **Fig. 11**, is shown in Fig. 12. In other words, the more perfect the structure is, the higher the exciton binding energy is. We have shown that the extent of aggregation (regardless whether J- or H-type) increases with the film thickness hence we expect the local energy minima to be deeper increasing thus the barrier for the exciton dissociation. From another point of view, the defects can also be considered as dissociation centres **[22,40]**. Furthermore, the defect state concentration N_D can be plotted as a function of the layer thickness as shown in **Fig. 13**a. Also in this case there is a change of the thickness dependence above 100 nm. The N_D- concentration decreases linearly from about 2 x $10^{16}cm^{-3}$ for the 49 nm thick layer to 6 x $10^{15}cm^{-3}$ for 126 nm and then it decreases gradually to 3 x $10^{15}cm^{-3}$ for 237 nm **[41].**

A correlation between the results of the ER-EIS and SPV measurements is shown in **Fig. 13**. The dependences of the defect state concentration (N_d) and the exciton diffusion length square (L^2) on the layer thickness in **Fig. 13**a was used to construct the graph in **Fig. 13**b. Besides direct pairs of measurements performed on samples of the same thickness (shown as full circles), the other points (empty circles with central dot) were obtained by the pairing of one experimental data point (either for N_d or L^2) from the graph 13a with its counterpart value being obtained by a straight line interpolation between the nearest data from the complementary dataset. It can be expected that the diffusion length square scales with the exciton lifetime and the carrier mobility (L^2 ~*Tji)* **[42]**. To simplify the problem, let us consider defect states as recombination centres. Then, the life time is inversely proportional to density of defects. Hence L^2 should be inversely proportional to the density of defects (L^2 ~ $1/N_d$) [**43**]. This conventional assumption, however, need not be true in its simple form over the whole range of the practical interest [**44**] which we checked having clear indications that the structure of the investigated polymer films depends on the film thickness. This is especially seen in the thicknesses dependence of the carrier mobility. Indeed, it can be seen even here that the

linear dependence in **Fig. 13**b changes its slope for the samples above 100 nm which is the same threshold thickness as emerging in all the other investigations in this article.

3.4. Grazing-incidence wide-angle X-ray scattering analysis

Grazing-incidence wide-angle X-ray scattering (GIWAXS) enables a straightforward estimation of the unit cell size parameters, its orientation, and texture with respect to sample surface. **Fig. 14**a shows a representative GIWAXS reciprocal space map of PTB7 sample with the thickness of 185 nm. The scattering pattern shows two partially oriented diffraction rings. The first one, located at the q = 0.33 $Å^{-1}$ with the highest intensity in the in-plane direction (along q_r) corresponds to the alkyl side chain spacing of 19 Å. The second one, with the highest intensity in the out-of-plane direction (along q_z) at the q = 1.7 $Å^{-1}$ origins from the n-n stacking distance of 3.7 Å. The spatial distribution of scattered X-ray intensity in reciprocal space confirms a preferential orientation of π-π stacking of PTB7 polymer chains parallel with the sample surface.

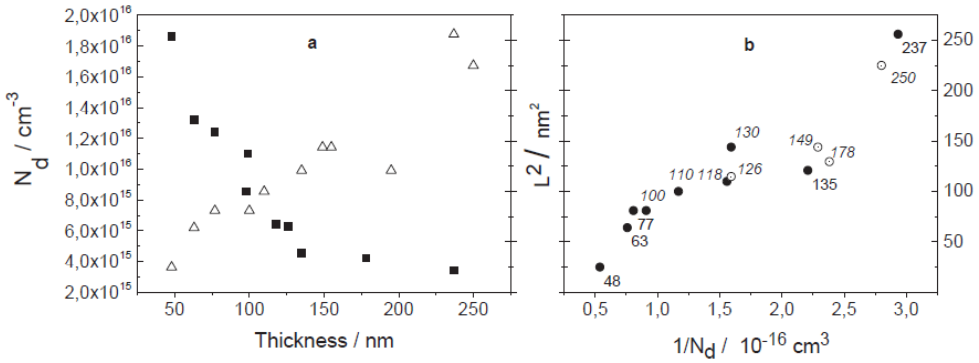

Fig. 13. a) The dependences of the defect state concentration (full squares) and the exciton diffusion length square (empty triangles) on the layer thickness; b) the dependence of the exciton diffusion length square on the $1/N_d$ (full circles stand for pairs of experimental points measured on the same sample thickness) supplemented with the interpolated data points (empty circles with central dot, for interpolation details see text). The labels show sample thickness in nm.

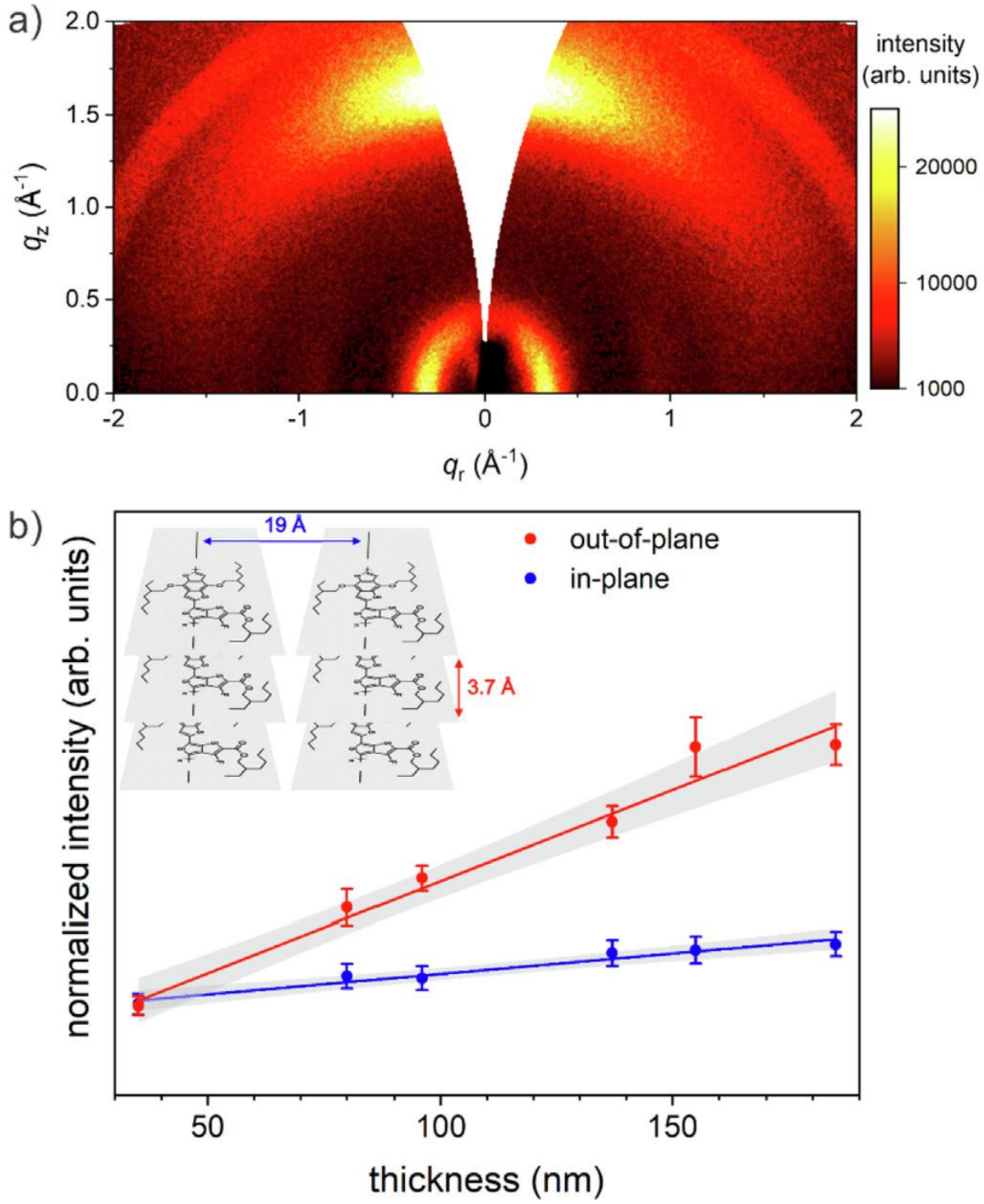

Fig. 14. a) GIWAXS scattering pattern of 185 nm thick PTB7 film. b) Normalized intensities of in-plane (blue) and out-of-plane (red) diffractions as a function of PTB7 film thickness. Inset shows schematically the "face-on" packing of PTB7 polymer. The π-π stacking and alkyl side chain spacing distances are shown in red and blue color, respectively.

Moreover, the symmetrical GIWAXS pattern suggests a uniaxial alignment of crystalline PTB7 domains with a random in-plane orientation of alkyl side chains. This orientation of conjugated polymers in thin film is often termed as the "face-on" configuration **[45]**.

In the following, we studied the evolution of crystalline order with the increasing thickness of spin-casted films. To quantify the crystalline phase, we integrated the in-plane and out-of-plane diffraction peaks in the x-ranges of < 0°,10° > and < 75°,105° > , respectively. Here the χ denotes the

angle between the transfer wavevector *q* and the surface normal. **Fig. 14**b shows the normalized intensity of in-plane and out-ofplane diffractions as a function of film thickness. With the increasing film thickness the intensity of out-of-plane diffraction is growing faster when compared to the intensity of in-plane diffraction. This suggest a preferential decrease of disorder along n-n stacking direction. In the theoretical framework, the π-π stacking in "face-on" configuration is equivalent to the formation of oriented H-aggregates **[46]**. Hence, the charge carrier mobility along the oriented n-n stacking direction should be positively influenced for thicker films. The experimental measurements of improved charge carrier mobility and exciton diffusion length for thicker films correlate well with the observed decreased disorder of n-n stacking in their "face-on" configurations.

3.5. The discussion of the driving force causing the observed thickness threshold phenomena

A strong correlation between the polymer film thickness and the development of the order in the film structure from nano to submicroscale has been shown according to the above discussed results, which are all consistent with each other and fit within a coherent picture with regards to the J-aggregate, H-aggregate, or HJ-aggregate formation varying with a change of thickness. Along with our previously published results **[21-24]** and the reports of other authors **[13,14,23,26-28]** the pertaining various materials, solvents, etc. we believe that the observed phenomena is of a general character and that there must be some driving force(s) dictating why and which given type of aggregate is likely to dominate the behaviour of the film and why there emerges a critical thickness of the film with regard to the structural order development. Moreover, we are convinced that the mechanism resulting in the observed behaviour is very general and common for all thin films cast from solutions, and that all of the overwhelming details concerning the specific influences of solvent choice, spin rate, time, temperature, and other processing conditions are of a secondary influence and can only moderate the main principal effect.

Thin films cast from polymer solutions may be found in a plethora of applications. The techniques of their preparation always rely on the key step of a thin liquid film drying. There are many experimental and practical approaches which resulted in successful film fabrication techniques. Moreover, a large number of theoretical descriptions of the process were introduced in order to achieve a quantitative and predictive understanding of the drying process in thin films **[47-52]**. The complexity of the available models limited their practical utilisation. There was a lack of an efficient and a robust modelling approach still covering all of the relevant physical parameters influencing the process. This challenge was addressed by the development of a minimal descriptive model based on physically meaningful parameters linked with observable variables showing an excellent agreement between the theory and the experiment **[53].** This novel analytical tool enables the description and treatment of the film drying problem within a four stage model. Here we note the original article by Hennessy et al. **[53]**, which also deals with the adsorption of solvent vapours by the thin film, but this is intentionally left aside in this discussion.

According to the analysis in Ref. **[53**], it is considered that the evaporating film is composed from a volatile solvent (solvent mixture) and at least one non-volatile solute (in this discussed case a polymer). Unlike quasi static conditions in simple blade coating or drying stationary films, the drying film experiences rotation during spin coating. However, if the attention is focused on the central area of the film neglecting radially dependent effects, a common approach can be accepted for all casting methods. The solution forms a 2D extended thin layer on top of a non-permeable substrate so there is no edge effect and the problem can be simplified to the one-dimensional one in the direction perpendicular to the substrate plane. The surface tension of the liquid is assumed to be large enough to prevent any deformations of the liquid surface from the perfect plane. Any wrinkling, waves, Marangoni phenomena or any other eventual instabilities are neglected. The finite thickness of the film *h* can be described by a function of the drying time *h(t)*. The diffusion is assumed as the

sole means of the mass transport within the film bulk and adequately described by the two Fick's laws using the diffusion coefficient *D* that is concentration dependent since it governs the diffusion process of solvent molecules starting from a dilute solution up to a solvent diffusion through to a dry polymer film. No convective transport or hydrodynamic effect is considered. The exchange of the solvent with the atmosphere is described using a mass transfer coefficient *k*. The diffusive flux at the solution film surface is balanced by the flux of the solvent vapour to the atmosphere. Any temperature gradients are assumed to be negligible and the density of the solvent, the solute and their mixture at any concentration is of the same value, hence taken as constant. The concentration of the solvent p is defined as volume %, however due to the aforementioned simplification (constant density of the solution and solute is the same as weight percent). The initial solvent concentration is denoted as p_i and for a fully dried film ($t \rightarrow \infty$), we assume $\varphi_\infty = 0\%$.

Supposing a solvent rich system containing only a few percent of the solute, which is a reasonable expectation for spin coating and other thin film preparation technologies, the drying proceeds in the following stages which are schematically depicted in **Fig. 15**. The first drying stage is characterised by the initial depletion of the solvent and the creation of a concentration profile which grows until it reaches the substrate.

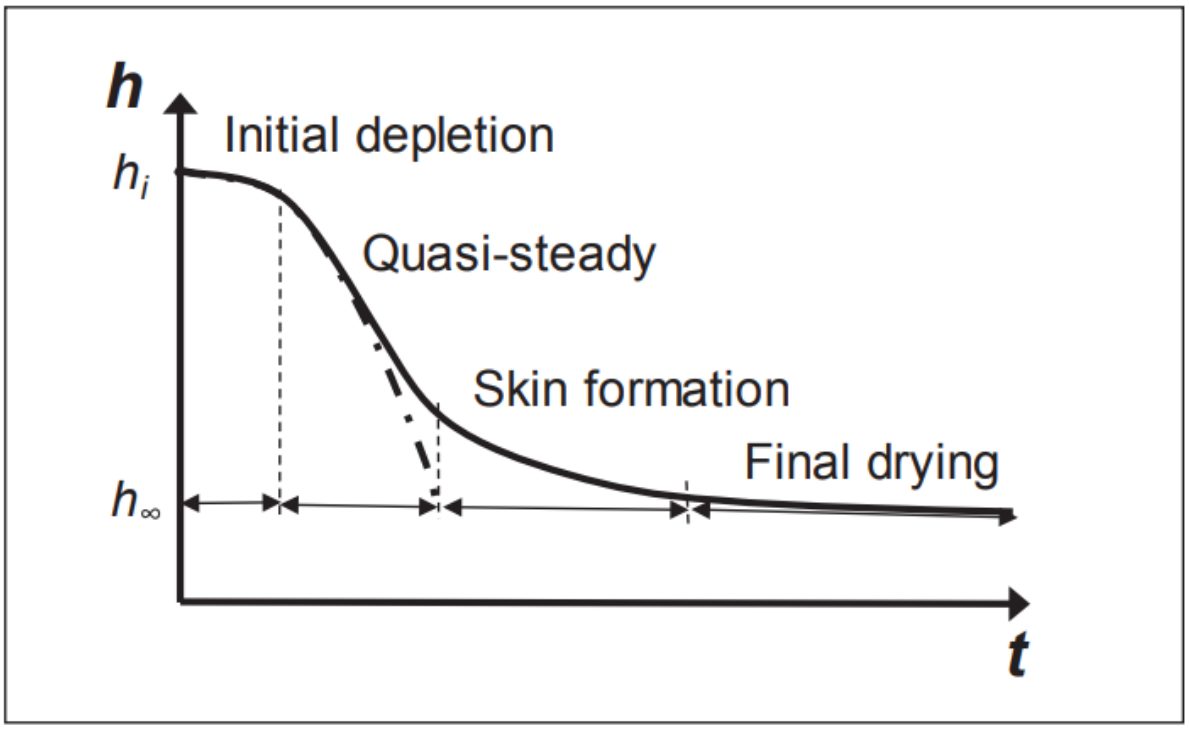

Fig. 15. The schematic diagram of stages during the thin film drying. The process is plotted with the relation of the dependence of the film thickness h to the time of drying *t*.

In that way, a concentration profile is formed with a small concentration of gradients across the film thickness which results in the second stage of drying which is characterised by a quasi-steady state condition. The solvent concentration decreases as the evaporation from the film proceeds. At this stage, the diffusion of solvent through the film is able to replenish the solvent evaporated and is transferred out from the film into the gaseous phase. This stage may continue until the film fully and quickly dries which is illustrated by the dash dot curve in **Fig. 15**. Alternatively, a third and fourth stage may develop as indicated by the solid line in **Fig. 15**. The first case occurs when the solvent diffusion overbalances the solvent transfer rate into the gas phase for the whole drying time. The other case occurs when the diffusion flow of the solvent through the film decreases too much and the mass transfer of vapours prevails. A solute rich skin forms on the surface of the liquid film, if the

concentration of the solvent at the surface and in its subsurface proximity decreases sufficiently to induce a large change in the diffusion coefficient which leads to the deceleration of the solvent diffusion, depriving the diffusion coefficient in a positive feedback. This is the third stage of film drying called skin formation. A large solvent concentration gradient is formed across the skin and the evaporation rate is significantly slower. This results in the retardation of the rate of drying. Moreover, the gradients in the solution below the skin become smaller and the polymer solute takes time to form the solid phase. Thus, structural order differences between the films dried with and without the skin formation must necessarily occur. We believe that this is the reason which is generally responsible for such phenomena. Moreover, the fourth stage occurs after the solidification (gelation) of the whole film, i.e. the diffusion coefficient becomes so small, that it can be considered to be constant again. During this phase, the residual solvent is removed from the film and its thickness decreases only a little. It is rational to expect, that the time before complete drying can be considered as an opportunity for the polymer to improve its structure in terms of polymer chain segment packing and movements, somewhat similarly as in the case of any solvent vapour annealing. On the other hand, fast drying without the skin formation results in a film with less ordered polymer structure.

The transition point between the second and third drying stage is a critical event that can be characterised by the Peclet number (*Pe*). This dimensionless criterion represents the ratio between the mass transfer rate and the diffusion rate. Unlike Hennessy et al. **[53]**, who analysed the process by modelling and leading the order of the solutions of differential equations, we analysed the transition between the two modes of drying with the help of the Peclet number solely. If the solvent diffusion prevails during drying, no skin is formed while the dominance of the mass transfer of the solvent vapours away from the surface yields skin formation.

The Peclet number represents the ratio of the diffusive time scale (fdiff) to the advection time scale ($-r_{mt}$). These time scales represent the reciprocals of the diffusion rate and the mass transfer rate, respectively, and it is expressed as follows:

$$Pe = \frac{rate\ of\ advection}{rate\ of\ diffusion} = \frac{\tau_{diff}}{\tau_{mt}} = \frac{\frac{h^2}{D}}{\frac{h}{k}} = \frac{kh}{D} \qquad (6)$$

In general, there are two approaches to the analysis by non-dimensional correlations. The first one is based on the initial estimates of the relevant parameters and it handles the criterion as one “global” number. The initial guess is then considered as a decisive characteristic for the whole process. In our case, this corresponds to the initial value *Pei* of the Peclet criterion,

$$Pe_i = \frac{kh_i}{D_i} \qquad (7)$$

in which the h_i is the initial thickness of the liquid film, *k* is the mass transfer coefficient and *D,* is the initial diffusion coefficient of the solvent in the polymer solution.

The other approach to the non-dimensional correlation problem solution is based on an analysis of the local and time variations of the criterion value. Due to the geometrical constraints and initial assumptions, the local value of *Pe* does not differ from the global value. However, the instantaneous value of *Pe* changes with the time of drying. To investigate which mode of drying will occur, it is not necessary to simulate the whole process but only the development of the value of the *Pe* number with the progression of the drying process. The three variables *k*, *h*, *D* need to be analysed.

The mass transfer coefficient *k* is a constant given by the assumption that the partial pressure difference between the air over the film surface and in ambient air is kept constant.

The thickness *h* of the drying film changes from its initial value h_i at the beginning of the drying process as a function of time h(t) however, it is more suitable if it is expressed with the help of *t*φ expressing thus the thickness as a function of the drying process progression h(φ). Moreover, when the φ is non-dimensionalised (p/p_i), it is possible to monitor the drying process progression on the scale from 1 (beginning of the drying) to 0 (for the fully dried film). Then the thickness is expressed as $h(\varphi/\varphi_i)$ and the thickness of the dry film h_{∞} corresponds to the concentration of the solute(s) in the solution.

$$h(\varphi) = h_i(1 - \varphi_i + \varphi) \tag{8}$$

$$h(\varphi/\varphi_i) = h_i\left(1 - \varphi_i + \frac{\varphi_i}{\varphi_i}\varphi\right) = h_i\left(1 - \varphi_i\left(1 - \frac{\varphi}{\varphi_i}\right)\right) \tag{9}$$

$$h_{\infty} = h_i(1 - \varphi_i) \tag{10}$$

It is well known that the diffusion coefficient (*D*) of solvents in polymers is dependent on the fraction of solvent in the system. The lowest value may be observed in diffusion of the solvent molecules through a dry polymer, which is actually the case of permeation. By increasing the swelling of the polymer, the diffusion coefficient increases up to the values common for polymer solutions. Then, an infinite dilute solution represents the upper limit of the diffusion coefficient value in the given solvent - solute system. The dependence of the diffusion coefficient on the solvent fraction *D*(φ) may be described as follows:

$$D(\varphi) = (D_0 - D_{\infty})\cdot\varphi^a + D_{\infty} \tag{11}$$

in which p is the solvent fraction, D_0 is the effective diffusion coefficient in a diluted solution while D_{∞} is the diffusion coefficient in the dry film and exponent *a* is a fitting parameter. This polynomial is considered as an adequate general description of the diffusivity dependence on the concentration **[54]**. In order to describe the diffusion coefficients independently to its absolute value, a non-dimensional parameter is introduced as the ratio:

$$\delta = \frac{D_{\infty}}{D_0} \tag{12}$$

in which δ is the non-dimensional diffusivity range.
With respect to further analysis, it is useful to define the limit initial value Pe_{i0} which represents the value of Pe, for an infinitely diluted solution using D_0:

$$Pe_{i0} = \frac{kh_i}{D_0} \tag{13}$$

The instantaneous value of Pe can be expressed with the help of pp or even better as a function of its non-dimensionalised form φ/φ_i:

$$Pe\left(\frac{\varphi}{\varphi_i}\right) = Pe_{i0}\cdot f\left(\frac{\varphi}{\varphi_i}\right) \tag{14}$$

which may be further developed as follows:

$$Pe = \frac{kh}{D} = \frac{kh_i(1-\varphi_i+\varphi)}{D_0((1-\delta)\varphi^a+\delta)} = \frac{kh_i}{D_0}\cdot\frac{(1-\varphi_i+\varphi)}{((1-\delta)\varphi^a+\delta)} = Pe_{i0}$$
$$\cdot\frac{(1-\varphi_i+\varphi)}{((1-\delta)\varphi^a+\delta)} = Pe_{i0}\cdot\frac{(1-\varphi_i+\frac{\varphi}{\varphi_i}\varphi_i)}{((1-\delta)(\frac{\varphi}{\varphi_i}\varphi_i)^a+\delta)} \qquad (15)$$

Hence, for any given limit initial value Pe_{i0} which is always a constant, the analysis of the problem is reduced to the analysis of the $f(\varphi/\varphi_i)$ term, expressed by:

$$f(\frac{\varphi}{\varphi_i}) = \frac{(1-\varphi_i+\frac{\varphi}{\varphi_i}\varphi_i)}{((1-\delta)(\frac{\varphi}{\varphi_i}\varphi_i)^a+\delta)} \qquad (16)$$

In order to examine the transition between skin-less and skin formation drying, typical reasonable situations characterized by a set of values of the parameters a, δ and **(doplnit symbol)**$_i$ are considered. The critical value of Pe is 1 thus properly chosen Pe_{i0} shall be < 1 because the $f(\varphi / \varphi_i)$ starts always at the value 1 for $\varphi = \varphi_i$ at the beginning of the thin film drying regardless of the values of a and φ.

The simplest first example assumes the diffusion coefficient to be a constant independent on the solvent concentration ($D_0 = D_\infty$ = const.) which also means that parameters a = 0 δ, **(doplnění symbolu)** = 1. The model results in a set of lines for the representative φ_i values resembling fan ribs starting from the point **[1,1]** in the graph in **Fig. 16**. Within this system, the skin formation will never occur if the value Pe_{i0} is properly chosen. Moreover, the value of $f(\varphi / \varphi_i)$ decreases linearly with the progression of drying $(1 - p/p_i)$. The line for $p_i = 0$ is a hypothetical limit for a dry film. Indeed, the graph of $\lim f(\varphi/\varphi_i)$ is a horizontal line indicating no change.

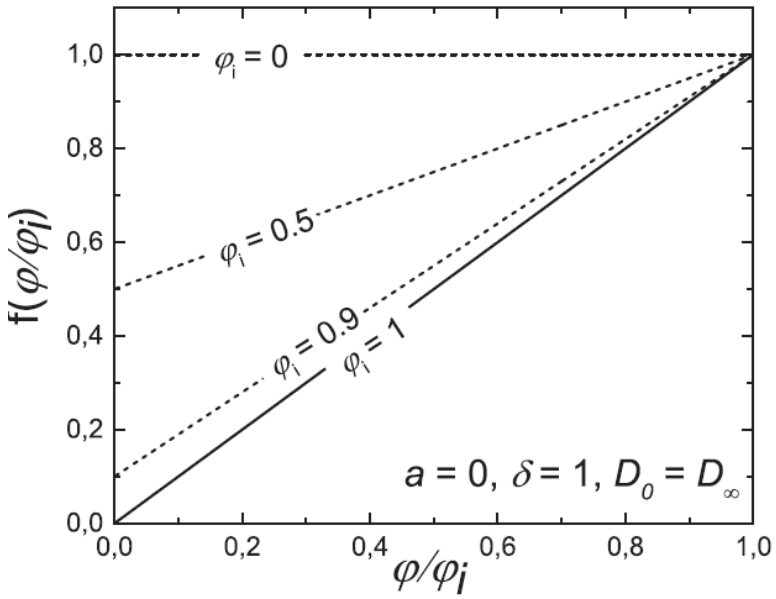

Fig. 16. The dependences off(p/pO on the p/p, values in the simplest case of film drying, in which a = 0 and S = 1.

Another extreme is the unity diagonal for φ, = 1 and δ = 1 which is added hereafter to all graphs for a comparison as an indication of the lowest limit case. Also this line is a mathematical construction

since for p, = 1 the actual value of p is always constant φ = φ, = 1 as the concentration of a pure solvent cannot by changed by drying.

The second example when *a* equals 1 which means that diffusion coefficient is a linear function of solvent concentration is modelled in **Fig. 17**. Four graphs are shown for the p, values selected from the range (0.995-0.9). Within each graph, a set of curves are shown for the δ values ranging from 10^{-5} to 0.1. This case represents the simplest (i.e. linear) dependency of the diffusion coefficient on the solvent concentration. The transition between the solutions which never form the skin and skin formatting solutions depends on the diffusivity range, i.e. parameter δ. For example, if $\delta > 0.01$ then all solutions with a starting polymer concentration of <0.01 will dry without skin formation. Moreover, the function $f(\varphi / \varphi_i)$ reaches a value of 2 for these initially low concentrated solutions for cases with S < 0.01 when the residual solvent concentration (p/p,) in the drying film is about 0.01. This indicates that the skin formation may be skipped easily for the diluted solutions even at a very low non-dimensional diffusivity range (e.g. shown for 10^{-5} in **Fig. 17**) if the value of Pe_{i0} is less than 0.5. For the solutions initially containing several percent of a polymer, that can by typically used for spin coating, a choice of the initial value of Pe_{i0} lower than 0.1 could completely assure a skin formation-less drying process. In the next example when a equals 2 which means that the diffusion coefficient is a quadratic function of the solvent concentration is modelled in **Fig. 18**.

Four graphs are shown for the φ_i values selected from the range (0.995-0.9) like in the previous case. Within each graph, a set of curves is shown for delta values ranging from 10^{-5} to 0.1. It can be seen that the curves representing the function $f(\varphi / \varphi_i)$ for specific parameters have a maximum amount. The position of the maximum is shifted to the low φ/ φ_i values, the smaller the parameter δ is the closer the position of the maximum is to zero. For example, if the value of Pe_{i0} is less than 0.1, the transition to the skin formation stage of drying may occur when the film dries to about 20% of its initial solvent concentration or less in all of the examined cases. However, the liquid film is most likely already in a form of a swollen gel in its whole volume and the eventual skin formation may not have such an important influence on the film structure formation as it would have in the case of an early transition to the skin formation stage when the liquid solution is covered by a solid skin surface. It can be said in other words that the film drying skips the skin formation stage and transits from the steady state drying directly into the final drying stage.

The dependences of the argument of the $f(p/p_i)$ function maximum and of the maximum value of the f(p/pi) function on the variable S are plotted in the range from 10^{-5} to 1 in **Fig. 19**. The solution was obtained by the differentiation of the equation **(16)** for *a* = 2, φ, was a parameter set to discrete values from 0.9 to 1. It can be seen from the left graph that the functional extremes for δ below 0.1 are achieved for ca. φ/φ, = 0.5 and for lower values, i.e., when the film contains less than 50% of solvent which means, the film is already just a swollen polymer rather than a liquid film. Once the film passes over the point of gelation during its drying, it can be expected that its structure will be much more restricted in its eventual organisation process due to the physical fixation of polymer chains by entanglement and the eventual skin formation will have a much less pronounced effect if it forms at all. The right graph tells for example that for $\delta = 0.001$ the maximum value of the $f (\varphi / \varphi,)$ function never exceeds ca. 100 for any reasonable (with respect to spin coating) polymer solution concentration which means that, for all of the values of Pe_{i0} smaller than 0.01 the skin will never be formed.

Based on both our experimental evidence and on the discussed theoretical model, the thickness *h* has the greatest importance in the film drying process because the transfer coefficient k is a constant and the diffusion coefficient D is either constant or is a function of h. If any final thickness of the prepared film has is desired, the initial thickness h_f is set by the concentration of the polymer solution used for the film preparation.

Fig. 17. The dependences of *f(<φ /< φi)***(doplnění symbolů)** on the *<p/<pi* values in the case of film drying, in which the diffusion coefficient is linear function of solvent concentration and *a* =1. **(doplnění symbolů)** on

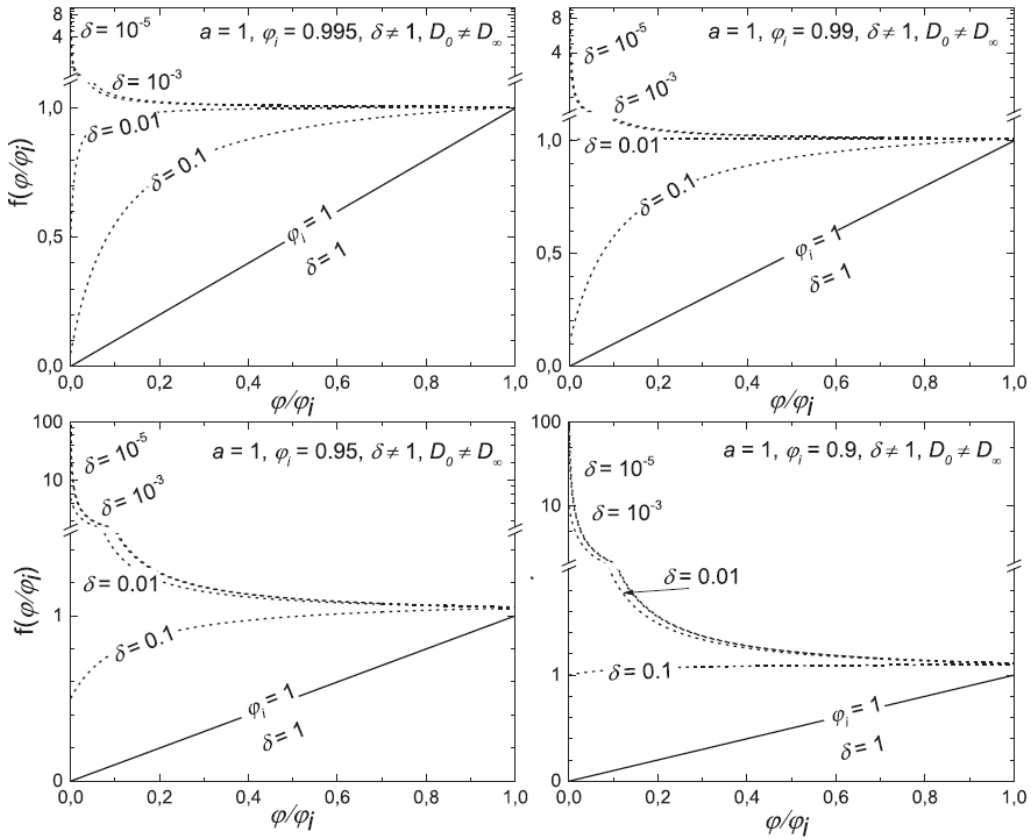

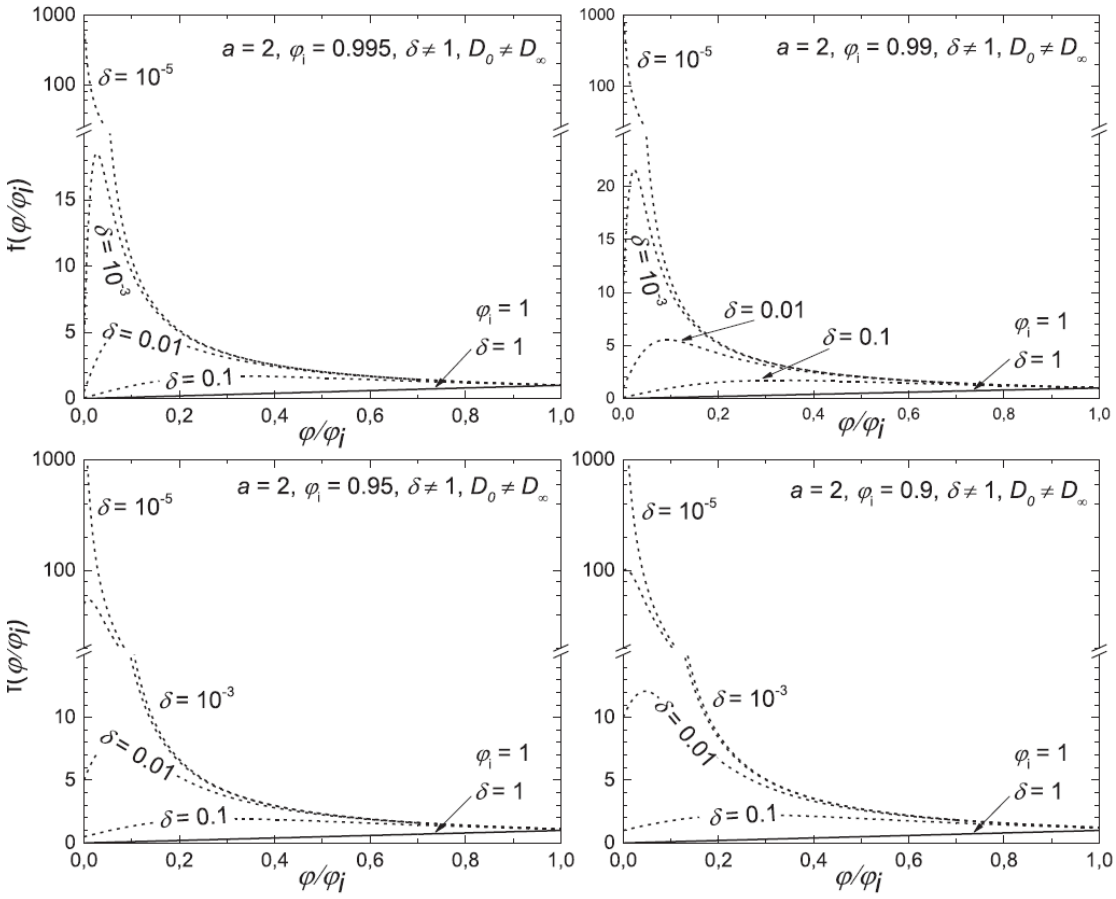

Fig. 18. The dependences of the *f(<φ /< φi)* on the ^/^i **(doplnění symbolů)** on values in the case of film drying, in which the diffusion coefficient is quadratic function of the solvent concentration and *a* = 2.

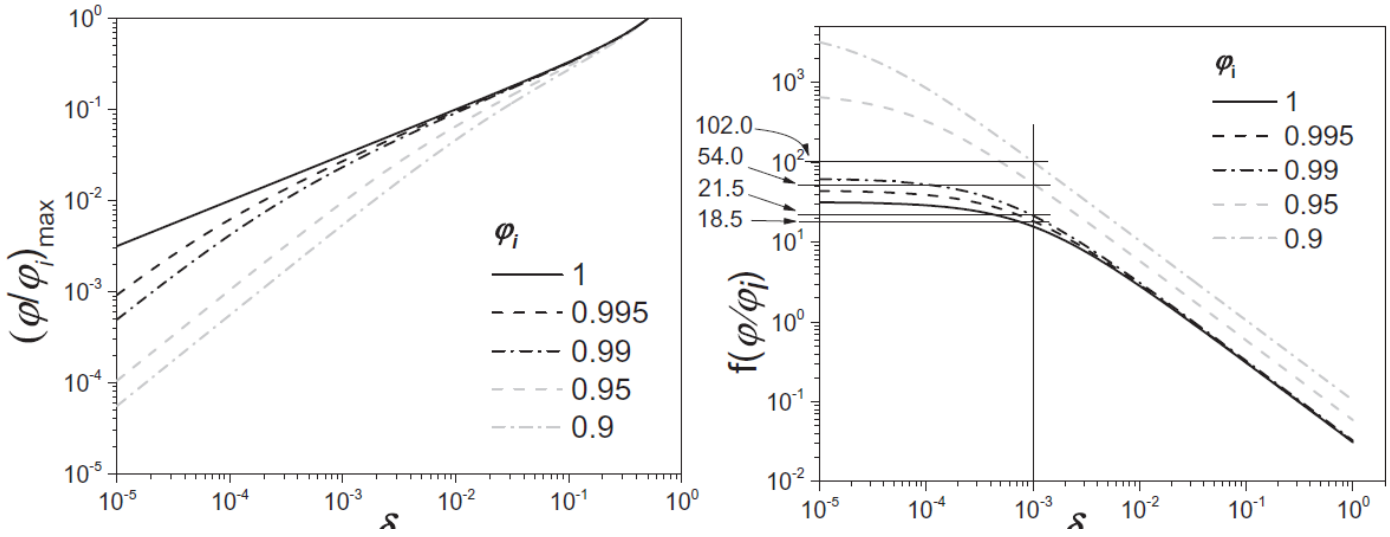

Fig. 19. The dependence of the maximum of the φ/ φi) **(doplnění symbolů)** on (left side) and the dependence of on the variable S.

Depending on the typical values of the diffusion coefficient (given by *D0, a,* and δ **(vložení symbolu)**), the drying conditions (given by k), and the initial thickness h_f and the concentration φ_i, thin films may be prepared with or without skin formation during film drying. However, under the given initial conditions (D_0, a, δ, k, φ_i) **(vložení symbolu)** there must exist a critical initial thickness h_i or in other words a desired threshold for the dry film thickness h_∞ which corresponds to the transition between skin formation-less and skin formation modes of the thin film drying. The skin formation during the

drying process is the most plausible explanation for the observed enhanced structural order development in the case of films thicker than the threshold thickness which was observed in the previous experimental works of our group and many other researchers too. We identify the transition between skin formation-less drying of thinner films and skin formation drying of thicker film as the mechanism of the described mesoscale effect.

4. Conclusions

In thin PTB7 films, all of the properties related to the absorption, the exciton formation, photoluminescence, the exciton diffusion length and carrier mobility, the width of the transport band gap, and defect concentration are strongly influenced by layer thickness. There exists a thickness threshold in all of the investigated aspects of the films at about 130 nm. We consider this complex phenomenon as a consequence of the mesoscale effect which emerges with the increase of the thickness of the polymer film due to more ordered microstructure, whereas the competition between the formations of J- and H-aggregates could arise.

From another point of view, it means that it is impossible to prepare films with a thickness varying over tens and hundreds nanometers with the same structure and physical properties. This has strong implications towards the general experimental praxis, e.g. the measurements of the exciton diffusion length based on photoluminescence quenching.

Moreover, the driving forces which are responsible for the described observations were theoretically analysed. The thin film drying may proceed with or without a polymer skin formation on the surface of a drying film. The occurrence of the skin formation stage depends on the initial conditions including the diffusion coefficient (and its dependence on the solute concentration), the drying conditions (given by the mass transfer coefficient), and the initial liquid film thickness and the solvent concentration. The transition between the skin formation-less drying for thinner films and skin formation drying for thicker films was explained with the help of the dimensionless Peclet number. We showed that for a polymer under given conditions there must exist a threshold for the initial thickness deciding which drying mode will occur and what kind of structural ordering will be therefore developed in the formed thin film. As the choice of the initial liquid film thickness is fully dependent on the desired dry film thickness at given solution concentration keeping all other conditions the same, the transition is straightforwardly manifested in the observed threshold thickness behaviour of the investigated films. This is the essence of the mesoscale effect experimentally observed so far.

References

[1] G. Yu, J. Gao, J.C. Hummelen, F. Wudl, A.J. Heeger, Polymer photovoltaic cells - enhanced efficiencies via a network of internal donor-acceptor heterojunctions, Science 270 (5243) (1995) 1789–1791.

[2] F. Bencheikh, D. Duche, C.M. Ruiz, J.J. Simon, L. Escoubas, Study of optical properties and molecular aggregation of conjugated low band gap copolymers: PTB7 and PTB7-Th, J. Phys. Chem. C 119 (43) (2015) 24643–24648.

[3] L.Y. Lu, L.P. Yu, Understanding low bandgap polymer PTB7 and optimizing polymer solar cells based on it, Adv. Mater. 26 (26) (2014) 4413–4430.

[4] Y.Y. Liang, Z. Xu, J.B. Xia, S.T. Tsai, Y. Wu, G. Li, C. Ray, L.P. Yu, For the bright future-bulk heterojunction polymer solar cells with power conversion efficiency of 7.4%, Adv. Mater. 22 (20) (2010) E135-+.

[5] I.H. Jung, W.Y. Lo, J. Jang, W. Chen, D.L. Zhao, E.S. Landry, L.Y. Lu, D.V. Talapin, L.P. Yu, Synthesis and search for design principles of new electron accepting polymers for all-polymer solar cells, Chem. Mater. 26 (11) (2014) 3450–3459.

[6] Y. Zhang, Q. Wan, X. Guo, W. Li, B. Guo, M. Zhang, Y. Li, Synthesis and photovoltaic properties of an n-type two-dimension-conjugated polymer based on perylene diimide and benzodithiophene with thiophene conjugated side chains, J. Mater. Chem. 3 (36) (2015) 18442–18449.

[7] Y. Li, Z. Xu, S.L. Zhao, D. Huang, L. Zhao, C.W. Zhang, J. Zhao, P. Wang, Y.Q. Zhu, Enhanced carrier dynamics of PTB7:PC71BM based bulk heterojunction organic solar cells by the incorporation of formic acid, Org. Electron. 28 (2016) 275–280.

[8] H.J. Park, H. Kim, J.Y. Lee, T. Lee, L.J. Guo, Optimization of polymer photovoltaic cells with bulk heterojunction layers hundreds of nanometers thick: modifying the morphology and cathode interface, Energy Environ. Sci. 6 (7) (2013) 2203–2210.

[9] U. Jeng, C.H. Hsu, H.S. Sheu, H.Y. Lee, A.R. Inigo, H.C. Chiu, W.S. Fann, S.H. Chen, A.C. Su, T.L. Lin, K.Y. Peng, S.A. Chen, Morphology and charge transport in poly(2- methoxy-5-(2 '-ethylhexyloxy)-1,4-phenylenevinylene) films, Macromolecules 38 (15) (2005) 6566–6574.

[10] Y.J. Lee, D.Y. Kim, P.F. Barbara, Effect of sample preparation and excitation conditions on the single molecule spectroscopy of conjugated polymers, J. Phys. Chem. B 110 (20) (2006) 9739–9742.

[11] J. Michl, R.G. Jones, W. Ando, J. Chojnowski (Eds.), Silicon Containing Polymers, Springer, 2000, pp. 499–529.

[12] T.J. Fauvell, T.Y. Zheng, N.E. Jackson, M.A. Ratner, L.P. Yu, L.X. Chen, Photophysical and morphological implications of single-strand conjugated polymer folding in solution, Chem. Mater. 28 (8) (2016) 2814–2822.

[13] F.C. Spano, C. Silva, H- and J-aggregate behavior in polymeric semiconductors, Annu. Rev. Phys. Chem. 65 65 (2014) 477–500.

[14] H. Yamagata, F.C. Spano, Interplay between intrachain and interchain interactions in semiconducting polymer assemblies: the HJ-aggregate model, J. Chem. Phys. 136 (18) (2012).

[15] S.H. Wang, S. Fabiano, S. Himmelberger, S. Puzinas, X. Crispin, A. Salleo, M. Berggren, Experimental evidence that short-range intermolecular aggregation is sufficient for efficient charge transport in conjugated polymers, Proc. Natl. Acad.Sci. U. S. A 112 (34) (2015) 10599–10604.

[16] M.A.T. da Silva, I.F.L. Dias, J.L. Duarte, E. Laureto, I. Silvestre, L.A. Cury, P.S.S. Guimaraes, Identification of the optically active vibrational modes in the photoluminescence of MEH-PPV films, J. Chem. Phys. 128 (9) (2008).

[17] J. Cornil, D. Beljonne, C.M. Heller, I.H. Campbell, B.K. Laurich, D.L. Smith, D.D.C. Bradley, K. Mullen, J.L. Bredas, Photoluminescence spectra of oligo-paraphenylenevinylenes: a joint theoretical and experimental characterization, Chem. Phys. Lett. 278 (1–3) (1997) 139–145.

[18] E. Hennebicq, G. Pourtois, G.D. Scholes, L.M. Herz, D.M. Russell, C. Silva, S. Setayesh, A.C. Grimsdale, K. Mullen, J.L. Bredas, D. Beljonne, Exciton migration in rigid-rod conjugated polymers: an improved Forster model, J. Am. Chem. Soc. 127 (13) (2005) 4744–4762.

[19] O.J. Dautel, G. Wantz, R. Almairac, D. Flot, L. Hirsch, J.P. Lere-Porte, J.P. Parneix, F. Serein-Spirau, L. Vignau, J.J.E. Moreau, Nanostructuration of phenylenevinylenediimide- bridged silsesquioxane: from electroluminescent molecular J-aggregates to photoresponsive polymeric H-aggregates, J. Am. Chem. Soc. 128 (14) (2006) 4892–4901.

[20] A. Alekseev, G.J. Hedley, A. Al-Afeef, O.A. Ageev, I.D.W. Samuel, Morphology and local electrical properties of PTB7:PC71BM blends, J. Mater. Chem. 3 (16) (2015) 8706–8714.

[21] P. Urbanek, I. Kuritka, S. Danis, J. Touskova, J. Tousek, Thickness threshold of structural ordering in thin MEH-PPV films, Polymer 55 (16) (2014) 4050–4056.

[22] P. Urbanek, I. Kuritka, Thickness dependent structural ordering, degradation and metastability in polysilane thin films: a photoluminescence study on representative sigma-conjugated polymers, J. Lumin. 168 (2015) 261–268.

[23] D.E. Yıldız, D.H. Apaydın, L. Toppare, A. Cirpan, Effect of layer thickness on the electrical parameters and conduction mechanisms of conjugated polymer-based heterojunction diode, J. Appl. Polym. Sci. 134 (2017), https://doi.org/10.1002/ app.44817.

[24] B. Hanulikova, I. Kuritka, P. Urbanek, Effect of backbone conformation and its defects on electronic properties and assessment of the stabilizing role of pi-pi interactions in aryl substituted polysilylenes studied by DFT on deca methyl(phenyl) silylene s, Chem. Cent. J. 10 (2016).

[25] I. Ben Khalifa, S. Bargaoui, A.H. Said, S. Ayachi, B. Zaidi, J. Wery, K. Alimi, About some properties of electro-synthesized short Oligo(Para-Fluoro-Anisole) (OPFA): a combined experimental and theoretical study, J. Mol. Struct. 997 (1–3) (2011) 37–45.

[26] T. Liang, Y. Makita, S. Kimura, Effect of film thickness on the electrical properties of polyimide thin films, Polymer 62 (2001) 6–10, https://doi.org/10.1109/TED.2015. 2476597.

[27] R.M. Overney, C. Buenviaje, R. Luginbuhl, F. Dinelli, Glass and structural transitions measured at polymer surfaces on the nanoscale, J. Therm. Anal. Calorim. 59 (1–2) (2000) 205–225.

[28] S.J. Benight, D.B. Knorr Jr., L.E. Johnson, P.A. Sullivan, D. Lao, J. Sun, L.S. Kocherlakota, A. Elangovan, B.H. Robinson, R.M. Overney, L.R. Dalton, Nanoengineering lattice dimensionality for a soft matter organic functional material, Adv. Mater. 24 (24) (2012) 3263–3268.

[29] J. Tousek, J. Touskova, A novel approach to the surface photovoltage method, Sol. Energy Mater. Sol. Cell. 92 (9) (2008) 1020–1024.

[30] G. Juska, K. Arlauskas, M. Viliunas, J. Kocka, Extraction current transients: new method of study of charge transport in microcrystalline silicon, Phys. Rev. Lett. 84 (21) (2000) 4946–4949.

[31] A.J. Mozer, N.S. Sariciftci, L. Lutsen, D. Vanderzande, R. Osterbacka, M. Westerling, G. Juska, Charge transport and recombination in bulk heterojunction solar cells studied by the photoinduced charge extraction in linearly increasing voltage technique, Appl. Phys. Lett. 86 (11) (2005).

[32] V. Nadazdy, F. Schauer, K. Gmucova, Energy resolved electrochemical impedance spectroscopy for electronic structure mapping in organic semiconductors, Appl. Phys. Lett. 105 (14) (2014).

[33] F. Schauer, V. Nádazdy, K. Gmucová, Electrochemical impedance spectroscopy for study of electronic structure in disordered organic semiconductors – possibilities and limitations, J. Appl. Phys. 123 (2018), https://doi.org/10.1063/1.5008830.

[34] F. Schauer, S. Nespurek, P. Horvath, J. Zemek, V. Fidler, Luminescence as a Tool for Crosslinking Determination in Plasma Polysilylenes Prepared from Organosilanes, (2000), pp. 321–325.

[35] A.J. Wise, J.K. Grey, Understanding the structural evolution of single conjugated polymer chain conformers, Polymers 8 (11) (2016).

[36] A.K. Thomas, H.A. Brown, B.D. Datko, J.A. Garcia-Galvez, J.K. Grey, Interchain charge-transfer states mediate triplet formation in purified conjugated polymer aggregates, J. Phys. Chem. C 120 (40) (2016) 23230–23238.

[37] Y. Liu, J. Zhao, Z. Li, C. Mu, W. Ma, H. Hu, K. Jiang, H. Lin, Aggregation and morphology control enables multiple cases of high-efficiency polymer solar cells, Nat. Commun. 5 (2014) 1–8, https://doi.org/10.1038/ncomms6293.

[38] K. Gmucova, V. Nadazdy, F. Schauer, M. Kaiser, E. Majkova, Electrochemical spectroscopic methods for the fine band gap electronic structure mapping in organic semiconductors, J. Phys. Chem. C 119 (28) (2015) 15926–15934.

[39] N. Vukmirovic, L.W. Wang, Density of states and wave function localization in disordered conjugated polymers: a large scale computational study, J. Phys. Chem. B 115 (8) (2011) 1792–1797.

[40] F. Schauer, I. Kuřitka, S. Nešpůrek, UV degradability of aryl-substituted polysilylenes, Polym. Degrad. Stabil. 84 (2004) 383–391, https://doi.org/10.1016/j. polymdegradstab.2003.11.011.

[41] T. Sato, H. Kinjo, J. Yamazaki, H. Ishii, 10(15) cm(-3) eV(-1) level detection of density of states of a p-type polymer by hv-dependent high-sensitivity ultraviolet photoemission spectroscopy, APEX 10 (1) (2017).

[42] C.A. Wolfgang Brutting, Physics of Organic Semiconductors, 2nd completely revised and enlarged edition ed. Wiley-VCH Verlag, 2012.

[43] A.S. Abramov, A.I. Kosarev, P.R.I. Cabarrocas, Kinetics of defects and electron, hole diffusion lengths during light soaking and consequent annealing, J. Non-Cryst. Solids 266 (2000) 419–422.

[44] R.H. Bube, D. Redfield, Kinetic and steady-state effects of illumination on defects in hydrogenated amorphous-silicon, J. Appl. Phys. 66 (2) (1989) 820–828.

[45] M.R. Hammond, R.J. Kline, A.A. Herzing, L.J. Richter, D.S. Germack, H.W. Ro, C.L. Soles, D.A. Fischer, T. Xu, L. Yu, M.F. Toney, D.M. Delongchamp, Molecular order in high-efficiency polymer/fullerene bulk heterojunction solar cells, ACS Nano 5 (2011) 8248–8257, https://doi.org/10.1021/nn202951e.

[46] V. Savikhin, L.K. Jagadamma, L.J. Purvis, I. Robertson, S.D. Oosterhout, C.J. Douglas, I.D.W. Samuel, M.F. Toney, Morphological, chemical, and electronic changes of the conjugated polymer PTB7 with thermal annealing, IScience 2 (2018) 182–192, https://doi.org/10.1016/j.isci.2018.03.002.

[47] A.F. Routh, Drying of thin colloidal films, Rep. Prog. Phys. 76 (4) (2013) 046603.

[48] K.E. Davis, W.B. Russel, An asymptotic description of transient settling and ultrafiltration of colloidal dispersions, Phys. Fluid. Fluid Dynam. 1 (1) (1989) 82–100.

[49] T. Narita, P. Hebraud, F. Lequeux, Effects of the rate of evaporation and filmthickness on nonuniform drying of film-forming concentrated colloidal suspensions, Eur. Phys. J. E 17 (1) (2005) 69–76.

[50] T. Okuzono, K. Ozawa, M. Doi, Simple model of skin formation caused by solvent evaporation in polymer solutions, Phys. Rev. Lett. 97 (13) (2006) 136103.

[51] P.-G. de Gennes, Solvent evaporation of spin cast films: ‘‘crust” effects, Eur. Phys. J. E 7 (1) (2002) 31–34.

[52] C. Peishi, D.C.T. Pei, A mathematical model of drying processes, Int. J. Heat Mass Transf. 32 (2) (1989) 297–310.

[53] M.G. Hennessy, G.L. Ferretti, J.T. Cabral, O.K. Matar, A minimal model for solvent evaporation and absorption in thin films, J. Colloid Interface Sci. 488 (2017) 61–71.

[54] I.H. Romdhane, R.P. Danner, J.L. Duda, Influence of the glass transition on solute diffusion in polymers by inverse gas chromatography, Ind. Eng. Chem. Res. 34 (1995) 2833–2840, https://doi.org/10.1021/ie00047a037.